Contents lists available at SciOpen

Food Science and Human Wellness

journal homepage: https://www.sciopen.com/journal/2097-0765

China Food Publishing Co.

Smartphone-assisted colorimetric sensor for selective detection of glyphosate residue in food based on analyte-enhanced laccase-like activity of cubic Ag_2O nanoparticles

Yue Tang[a,b], Linghui Huang[b], Jian Su[c], Zhen Wu[b], Lian Xia[b], Xiaojuan Niu[a,*], Yuangen Wu[b,*]

[a] College of Life Sciences, Guizhou Normal University, Guiyang 550025, China
[b] Guizhou Province Key Laboratory of Fermentation Engineering and Biopharmacy, School of Liquor and Food Engineering, Guizhou University, Guiyang 550025, China
[c] Wuliangye Yibin Co., Ltd., Yibin 644000, China

ARTICLE INFO

Article history:
Received 1 June 2024
Received in revised form 25 July 2024
Accepted 20 September 2024

Keywords:
Food analysis
Pesticide residue
Nanozyme
RGB (red, green, blue) recognition
Visual detection

ABSTRACT

Glyphosate is widely used in agriculture, and its residues accumulate in soil and water, which adversely affects human health. The existing colorimetric methods for glyphosate detection are usually achieved by inhibiting the catalytic activity of natural enzymes or nanozymes, and often require the participation of easily decomposable H_2O_2, leading to unstable detection capabilities or even false positive results. This article reports a smartphone-assisted sensor for colorimetric detection of glyphosate in several food samples based on enhancing the laccase-like activity of cubic Ag_2O nanoparticles. Glyphosate can significantly enhance the generation of radicals and electron transfer in cubic Ag_2O reaction solution, causing an obvious change in the color of the system, which can be easily distinguished by naked eye. The established sensor has excellent detection performance, with limit of detection as low as 2.09 μg/L, and it is highly selective to other competitive substances. The method of enhancing the enzyme-mimic activity of nanomaterials to detect glyphosate residues is proposed for the first time, which can avoid false positive results caused by traditional enzyme inhibition methods and complex food matrices. Moreover, smartphones can simplify the conventional analysis procedure and achieve convenient on-site monitoring of glyphosate pesticides in food.

1. Introduction

Glyphosate, as a commonly used herbicide with high efficiency and low toxicity, has been extensively applied in agriculture, landscaping and aquaculture[1-3]. However, the misuse of glyphosate in agriculture can lead to its residues accumulating in soil and water, adversely affecting the environment[4] and thereby endangering human health[2]. It has been reported that glyphosate pesticide has certain reproductive toxicity and teratogenicity, which can get into the human body *via* respiration and contact[5-6]. Meanwhile, the World Health Organization and the International Agency for Research on Cancer have listed glyphosate as a potential carcinogen to humans recently[7]. Therefore, many institutions have established maximum limits for glyphosate in food. For example, the Chinese Ministry of Agriculture has set a maximum allowable limit of 0.5 mg/kg for glyphosate residues in in vegetables and fruits[8], and the US Environmental Protection Agency has established a maximum tolerance limit of 700 μg/L for glyphosate residues in drinking water[9]. Therefore, the establishment of highly sensitive detection method for glyphosate is very important to ensure the safety of food.

Instrumental methods such as gas chromatography[10], tandem mass spectrometry[11], and liquid chromatography[12] are the most

* Corresponding authors.
Email address: 252984899@qq.com (X.J. Niu); wuyg1357@163.com (Y.G. Wu)
Peer review under responsibility of Beijing Academy of Food Sciences.

SciOpen Publishing services by Tsinghua University Press

http://doi.org/10.26599/FSHW.2024.9250401

reliable and frequently utilized methods for pesticide residue detection. Although these methods can provide reliable results and high sensitivity, they still have inevitable limitations in practical applications, such as complex instrument requirements, cumbersome operation steps, high analysis costs, and time-consuming processes. In addition, surface-enhanced Raman spectroscopy (SERS) with ultrasensitively has also been proposed for the monitoring of glyphosate residues[13]. But its stability and reproducibility are poor, which may affect the accuracy of detection. Recently, rapid detection methods such as fluorescence[14] and electrochemical methods[15-16] have also been utilized for pesticide detection like glyphosate, which have excellent detection performance. However, they often demand cumbersome electrode processing and may even use toxic fluorescent substances. In recent years, colorimetric method has been widely concerned by researchers. Compared with instrumental, fluorescent and electrochemical methods, colorimetry is more convenient and rapid, and the results can be directly observed[17-18].

Recently, researchers have paid great attention to nanomaterials with catalytic activity (referred to as nanozymes)[19-21]. Nanozymes with enzyme-mimic activities such as oxidase, peroxidase and catalase have been discovered successively[22-25]. Currently, the pesticide colorimetric detection methods based on nanozymes most rely on the color change of gold nanoparticles (NPs)[26] or the enzyme-mimic activity of peroxidase[27], which are highly susceptible to environmental influences and lead to unreliable detection results. Thus, the development of a new method for colorimetric detecting pesticides utilizing new enzyme-mimic activity is of great significance. Laccase is a type of polyphenol oxidase widely present in various plants, named after its discovery in lacquer trees[28]. Since only oxygen is required in the catalytic oxidation process, laccase has been favored by researchers recently[29-33]. Due to the fact that H_2O_2 is not involved in the react process of laccase, which enables us to obtain more accurate detection results. Therefore, we believe that laccase can supply a relatively stable sensing signal for the detection of pesticide residues like glyphosate. Furthermore, present strategies for detecting glyphosate residues based on nanozymes mostly depend on inhibiting their catalytic activity. However, there are many interfering substances in the biological environment, which can easily interfere with the accuracy of the detection. Therefore, establishing an analytical method to enhance the activity of laccase can increase the results exactitude of pesticide detection.

Herein, it is firstly found that glyphosate can directly enhance the laccase-like activity of Ag_2O NPs, which change the color of the system from light pink to deep red. This enables us to propose a novel sensor for glyphosate colorimetric determination by using the laccase-like activity of cubic Ag_2O NPs. The degree of red change in reaction solution is not only linearly related to glyphosate quantity, but also can be transformed into RGB (red, green, blue) values through software on smartphones, thereby achieving convenient quantitative detection of pesticide residues. This study is the first to report a new strategy for detecting pesticide residues by enhancing the activity of laccase, which can avoid false positive results caused by traditional enzyme inhibition methods and complex food matrices. Moreover, the proposed colorimetric sensor does not require H_2O_2 to be involved in the detection procedure, and is expected to be used for accurate measurement of pesticide in food.

2 Materials and methods

2.1 Reagents

Glyphosate, malathion, 2,4-dichlorophenol (2,4-DP), isocarbophos, dimethoate, acrylamide, sodium acetate, omethoate, iprobenfos, ammonia ($NH_3 \cdot H_2O$), trichlorfon, carbendazim, paraquat, acetamiprid, 4-aminoantipyrine (4-AAP), carbaryl, λ-cyhalothrin, parathion-methyl, agarose, acetic acid (HAc), dichlorvos, sodium hydroxide, potassium chloride, chlorpyrifos, methanol, silver nitrate ($AgNO_3$) powder and ethanol absolute are bought from Shanghai Aladdin Biochemical Technology Co., Ltd. (China). The soybean and orange juice used in the real samples bought from food market. The experimental water is all ultrapure water.

2.2 Instruments

The morphological characteristics of cubic Ag_2O NPs is observed by the scanning electron microscope (Sigma300, ZEISS). The electrophoresis analysis is performed by BEP-600 electrophoresis apparatus (Bertrand, Beijing, China). The X-ray photoelectron spectroscopy (XPS) (Nexsa, USA) is utilized to analyze the elements and groups of Ag_2O NPs. The purity of the Ag_2O crystals is measured through the X-ray diffraction (XRD) (6100, Japan). The JES FA200 Electron Spin-Resonance Spectrometer is utilized to collect the electron spin-resonance spectroscopy (EPR) signal. The Zeta potential and particle size of Ag_2O NPs are determined by a nanoparticle size and Zeta-potential analyzer (Beckman Coulter, USA). The absorbance values are recorded by the microplate spectrophotometer (US thermoelectric). The surface area analysis and pore size distribution of Ag_2O are obtained by ASAP 2020 Plus (Micromeritics, USA) specific surface and pore analyzer. The Fourier transform infrared spectroscopy (FTIR) was performed by a Nicolet 6700 FTIR spectrometer with a secondary Nicolet of 5th module (Thermo Scientific, USA) at a resolution of 1 cm^{-1} using KBr as a reference.

2.3 Preparation of cubic Ag_2O NPs

The preparation method of the cube-shaped of Ag_2O NPs is as follows[34]. Add 100 mL ammonia (0.01 mol/L) to 50 mL $AgNO_3$ (0.01 mol/L) solution while stirring. After mixing thoroughly, continue to stir for 20 min, and then continue to slowly drop 5 mL sodium hydroxide (0.1 mol/L) solution in the stirred state. Thus, a large amount of sediment appears in the container. Then the solution is centrifuged to obtain the precipitate, and the Ag_2O powder is obtained by drying the precipitate.

2.4 Electrophoresis and free radical analysis

After incubation for 30 min at 37 ℃, the samples with different ingredients are identified by 3.5% agarose gel electrophoresis at 85 V[35]. A certain amount of Ag_2O, 2,4-DP and glyphosate are mixed, and the semiquinone radicals in the reaction system is determined by EPR detector[36-37].

2.5 Catalytic kinetics of cubic Ag_2O NPs

Different contents of 5 μL Ag_2O (2 mg/mL) and 20 μL glyphosate pesticide are added into centrifuge tubes and blended evenly. Subsequently, 10 μL phenolic substrate 2,4-DP of different quantities, 415 μL buffer, and 50 μL chromogenic substrate 4-AAP (1 mg/mL) are added to the above mixture and thoroughly mixed. Put 200 μL of the above reaction solution into the enzyme-labeled plate, and measure the absorbance value of solution at 510 nm every 10 s. The reaction rate is calculated by Lineweaver-Burk formula, and the apparent kinetic parameters are obtained by Origin mapping. The extinction coefficient (α) of the oxidation product is known to be 13.6 L/(mmol·cm)[38].

2.6 Procedure of glyphosate detection

A certain amount of Ag_2O, glyphosate is put into the centrifuge tube and mix sufficiently. Then, 10 μL 2,4-DP, a certain volume of HEPES buffer and 4-AAP are added to form a 500 μL catalytic system. The color of the solution in the centrifuge tube is directly observed with the human eye, and the absorbance values at 510 nm of the experimental group (A_1) and the blank group (A_0) are measured. The blank group uses ultrapure water instead of glyphosate solution. The response of the constructed colorimetric sensor to glyphosate pesticide is determined by the difference of absorbance ($\Delta A = A_1 - A_0$). In addition, the procedures for detecting glyphosate pesticides using a smartphone are as follows. After a smartphone takes a picture of the reaction system under a fume hood with a fixed light source, and then the RGB values in the picture are converted through the Coloree software. Finally, input the obtained RGB values into the established standard curve to calculate the amount of glyphosate.

2.7 Analysis of actual samples

Taking into account the food contamination of glyphosate with different degrees, we chose tap water, soybean, orange juice, apple and tea leaf as the food samples to validate the detection performance of the proposed sensor in real samples. The pre-treatment process of food samples is referred to reported literatures. For tap water samples[39], the samples are filtered with filter paper to remove some suspended solids. Then, various quantities of glyphosate are added to tap water filtrate. Finally, microporous filter membrane (0.22 μm) is used to remove the microorganisms from the tap water to obtain the treated samples. For the soybean sample[14], 10 g of soybean powder is dissolved in 50 mL of water and mix thoroughly. Then glyphosate with various contents is added to the solution and ultra-sounded for 30 min. The solution is centrifuged at 5 000 r/min for 10 min to obtain the supernatant. The supernatant is mixed with methylene chloride and centrifuged for 5 min to remove the fat. Finally, the supernatant is diluted with buffer, and the filtrate is collected by microporous filter membrane filtration. Different amounts of glyphosate are added to orange juice to obtain a labeled sample[40]. The sample is then repeatedly filtered with microporous filter membrane until the solution becomes transparent and collected for detection. For the apple and tea leaf sample[35], different amounts of glyphosate were evenly sprayed on the surface of the samples. After drying in a fume hood for 12 h, the samples were repeatedly eluted with HEPES buffer, and then the eluate was filtered through a microporous filter membrane for further determination. Moreover, the content of glyphosate in the filtrate is measured with high performance liquid chromatography to validate the reliability of the constructed sensor.

3 Results and discussion

3.1 Characterization of cubic Ag_2O NPs

The morphology characteristics of nanomaterials are characterized by scanning electron microscope (SEM, Fig. 1A) and transmission electron microscope (TEM, Fig. 1B), Ag_2O exhibits a smooth cubic shape with a lateral size range of 150−400 nm (Fig. 1C). The crystal structure of Ag_2O is studied through XRD pattern (Fig. 1D). Distinct diffraction peaks can be observed at 32.79°, 38.07°, 54.90°, 65.44° and 68.76° from in Fig. 1D, which correspond to the (111), (200), (220), (311) and (222) reflection surfaces of Ag_2O, respectively[34,41]. All diffraction peaks in the figure are consistent with the results of Ag_2O (JCPDS No.41-1104), and there are no other impurity peaks. The results suggest that the prepared cubic Ag_2O NPs is well-crystallized. To further study the surface characteristics of Ag_2O, the experiment of nitrogen adsorption and desorption was carried out (Fig. 1E). The adsorption isotherm of cubic Ag_2O is consistent with the typical IV isotherm, and an obvious H1 type hysteresis loop appears in the range of 0.15−1.0 P/P_0, which proved that the surface of the Ag_2O displayed a relatively uniform pore structure. The analysis also proves that Ag_2O has a specific surface area of 2.83 m^2/g and an average pore size of 6.31 nm, which confirms that the as-prepared Ag_2O has the characteristics of mesoporous nanomaterial (2 nm < pore size < 50 nm).

The XPS further analyzes the elemental composition and chemical state of the nanomaterials, and the spectral diagram in Fig. 1F confirms the existence of Ag and O elements. The Ag 3d spectrum (Fig. 1G) can be divided into 2 peaks at 368.1 and 374.1 eV, respectively corresponding to $3d_{5/2}$ and $3d_{3/2}$ of Ag, and 2 fitted peaks are attributed to Ag^+. Similarly, the spectrum of O 1s is also divided into 2 fitted peaks (Fig. 1H). According to previous literature[42], the strong peak at the binding energy of 531.0 eV corresponding to the Ag−O bond, suggesting that the exist of bound oxygen on the surface of Ag_2O. And the weak peak of 529.6 eV may be attributed to the sorption of hydroxyl groups on the surface of Ag_2O. All of the above demonstrate that Ag_2O NPs with a cubic structure have been successfully prepared. Moreover, Ag_2O can soluble in water to form a stable colloidal solution with obvious Tyndall effect (Fig. S1).

3.2 Construction of colorimetric sensor

3.2.1 Principle of sensor

It is firstly found that glyphosate pesticide can enhance the laccase-like activity of Ag_2O NPs. Therefore, a simple and reliable colorimetric sensor for glyphosate is constructed, and the detection principle is shown in Fig. 2. The cubic Ag_2O NPs can oxidize phenolic substrate 2,4-DP to produce semiquinone radical, while molecular oxygen as an electron acceptor generates corresponding free radical and is further reduced to water molecules[41]. Then, the semiquinone radical generated in the reaction solution will react with the added chromogenic agent 4-AAP, ultimately producing a pink substance

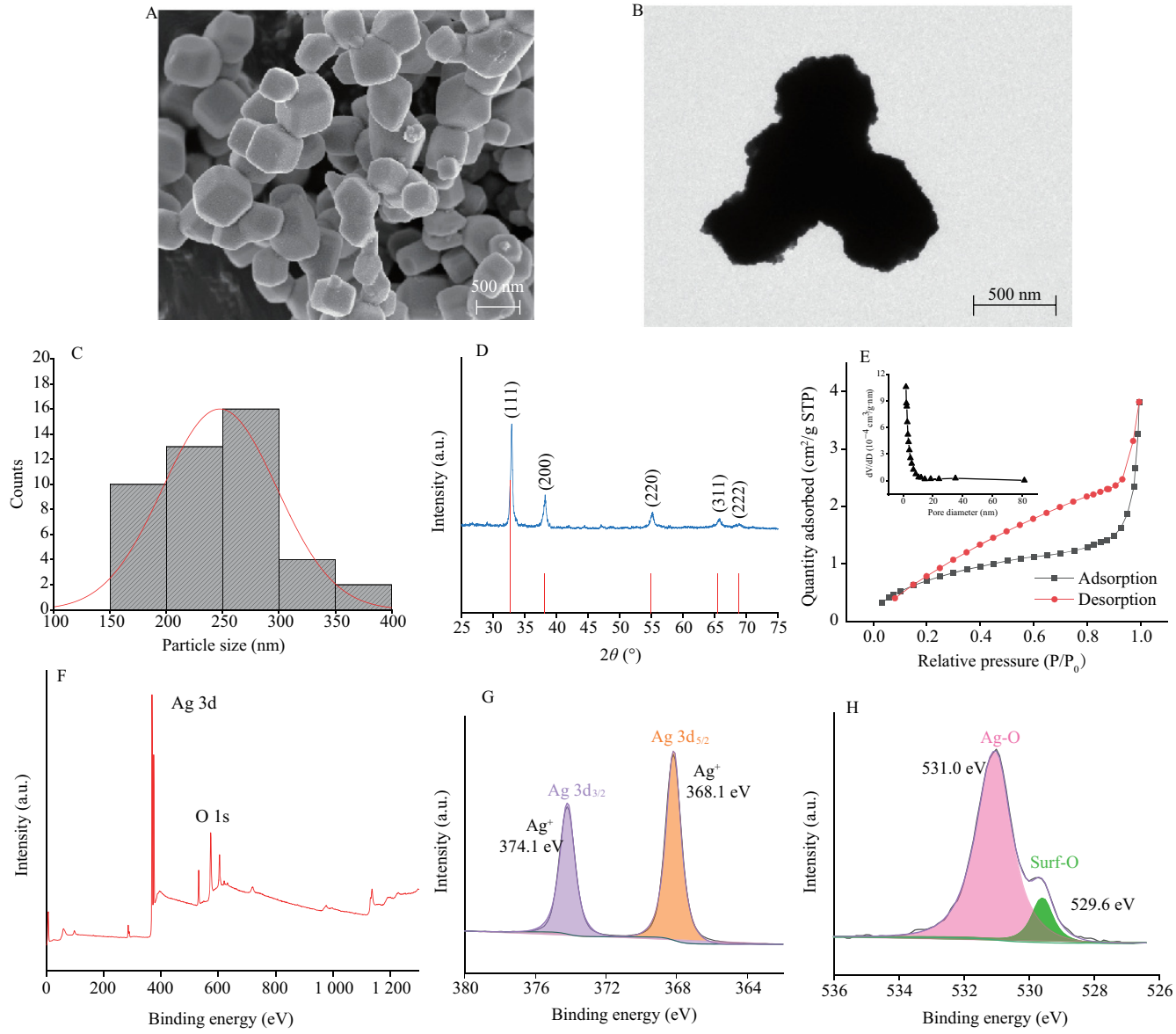

Fig. 1 (A) SEM image of cubic Ag_2O NPs. (B) TEM image of cubic Ag_2O NPs. (C) Size distribution histogram of cubic Ag_2O NPs. (D) XRD pattern of cubic Ag_2O NPs. (E) Nitrogen adsorption and desorption isotherms of Ag_2O. Inset: corresponding pore-size analysis. (F) XPS pattern of cubic Ag_2O NPs. (G) Ag 3d high-resolution XPS spectra of cubic Ag_2O NPs. (H) O 1s high-resolution XPS spectra of cubic Ag_2O NPs.

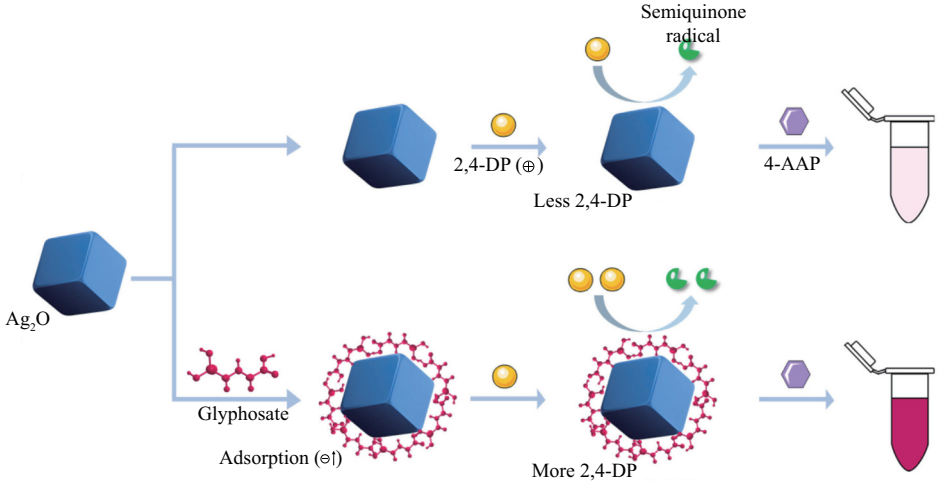

Fig. 2 Schematic diagram of detecting glyphosate with colorimetric sensor.

with a weak absorption peak at 510 nm (Fig. S2). Once glyphosate is added, pesticide molecules adsorb onto the surface of Ag_2O NPs to generate glyphosate-Ag_2O compounds with enriched negative charges. Thus, the complex attracts a large number of opposite-charged 2,4-DP close to the Ag_2O NPs by electrostatic adsorption and then catalyzes them. Finally, the reaction system produces a large number of red products, showing a deep red color. The degree of red variation in the catalytic solution is linear with the pesticide content, which enables us to establish a novel sensor for colorimetric detection of glyphosate.

3.2.2 Feasibility of sensor

The feasibility of the established colorimetric sensor for the detection of glyphosate pesticide is evaluated by observing and measuring the absorption spectra of reaction systems containing different substances (Fig. 3A). The cubic Ag_2O NPs have the laccase-like activity and indeed can catalytic oxidize phenolic 2,4-DP to generate semiquinone radicals, the latter react with 4-AAP to produce a small amount of red product. Then, the solution appears pink and produces a weak peak at 510 nm (Sample 1). Once adding various quantities of glyphosate into the reaction solution, the nanozymes can oxidize a large amount of 2,4-DP to produce radicals. Thus, the system appears deep red and produces a distinct absorption peak at 510 nm (Samples 2−4). However, both the substrate alone and the substrate containing glyphosate are colorless and have no characteristic absorption peaks (Samples 5−6). There is a positive correlation between the color variation in solution and the content of pesticide molecule, which can be applied to the colorimetric determination of glyphosate in food. Furthermore, the effects of different substances in the solution on the sensor are recorded (Fig. S3). All solutions appear colorless, indicating that they do not affect the sensor. The absorbance values of the Ag_2O catalytic system containing different substances at different times are determined to obtain the best reaction time (Fig. 3B). Regardless of whether glyphosate solution is added, the absorbance value of the cubic Ag_2O NPs catalytic system increases with the raise of reaction time until it reaches saturation at 20 min. In view of the need to detect the pesticide rapidly, the 15th min is chosen as the collection time for the follow-up experiments.

3.3 Enhancement mechanism of glyphosate on Ag_2O NPs

3.3.1 Electrophoresis and Zeta potential analysis

To validate the interaction between glyphosate and cubic Ag_2O NPs, agarose gel electrophoresis experiments are conducted. As shown in Fig. 4A, the injection hole of the first channel presents the inherent black brown color of Ag_2O NPs, which is due to the serious aggregation of nanozymes in the electrophoresis process and the inability to passing the holes formed by the gel. Surprisingly, the injection holes in second channel appear light gray with brown bands on the gel. This can be attributed to the fact that the cubic Ag_2O NPs are more dispersed after the interaction with glyphosate and can migrate on the agar-gel, thus leaving fewer nanozymes in the vicinity of the sample pore. The data imply that glyphosate can adsorb on the surface of Ag_2O NPs and improve their dispersibility.

To further verify the adsorption between glyphosate and Ag_2O NPs, the Zeta potential of the nanozymes front and back the addition of pesticide is measured (Fig. 4B). The potential of individual Ag_2O is −9.74 mV, while the potential of the nanozymes solution with added glyphosate pesticide is −14.34 mV. This is mainly due to the adsorption of negatively charged glyphosate[43] on the surface of Ag_2O NPs, forming complexes with enriched negative charge. The above results show that glyphosate pesticide can be adsorbed on the surface of cubic Ag_2O NPs to generate low potential compounds, and making the nanozymes solution more dispersed. In addition, the 2,4-DP solution is positively charged.

3.3.2 FTIR analysis

To further investigate the interaction mechanism between Ag_2O and glyphosate, the FTIR spectra of Ag_2O before and after the addition of glyphosate were recorded. As exhibited in Fig. 4C, the FTIR spectrum of Ag_2O was consistent with previous reports[44-50]. The observation of bands (1 060, 883, 815, 695 and 600 cm^{-1}) from 600−1 100 cm^{-1} are attributed to Ag−O stretching vibration and thereby confirming the formation of the Ag_2O NPs. For the spectrum of Ag_2O after reaction with glyphosate, the obvious peaks at 3 386 and 1 656 cm^{-1} were ascribed to the stretching vibration of O−H, indicating

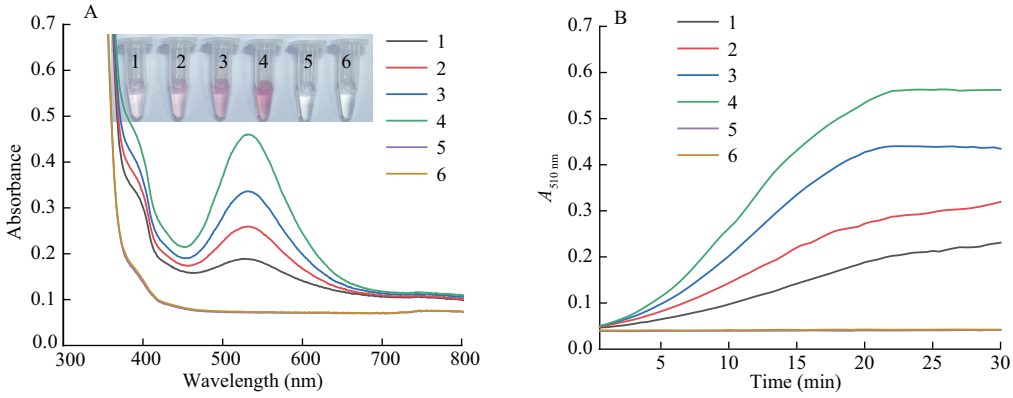

Fig. 3 (A) Visual pictures and absorption spectra of varying catalytic solutions and (B) the consequential absorbance values at various reaction times. Sample 1, cubic Ag_2O NPs + 2,4-DP + 4-AAP; Sample 2, Sample 1 + 40 μg/L glyphosate; Sample 3, Sample 1 + 200 μg/L glyphosate; Sample 4, Sample 1 + 400 μg/L glyphosate; Sample 5, 2,4-DP + 4-AAP; Sample 6, Sample 5 + 400 μg/L glyphosate.

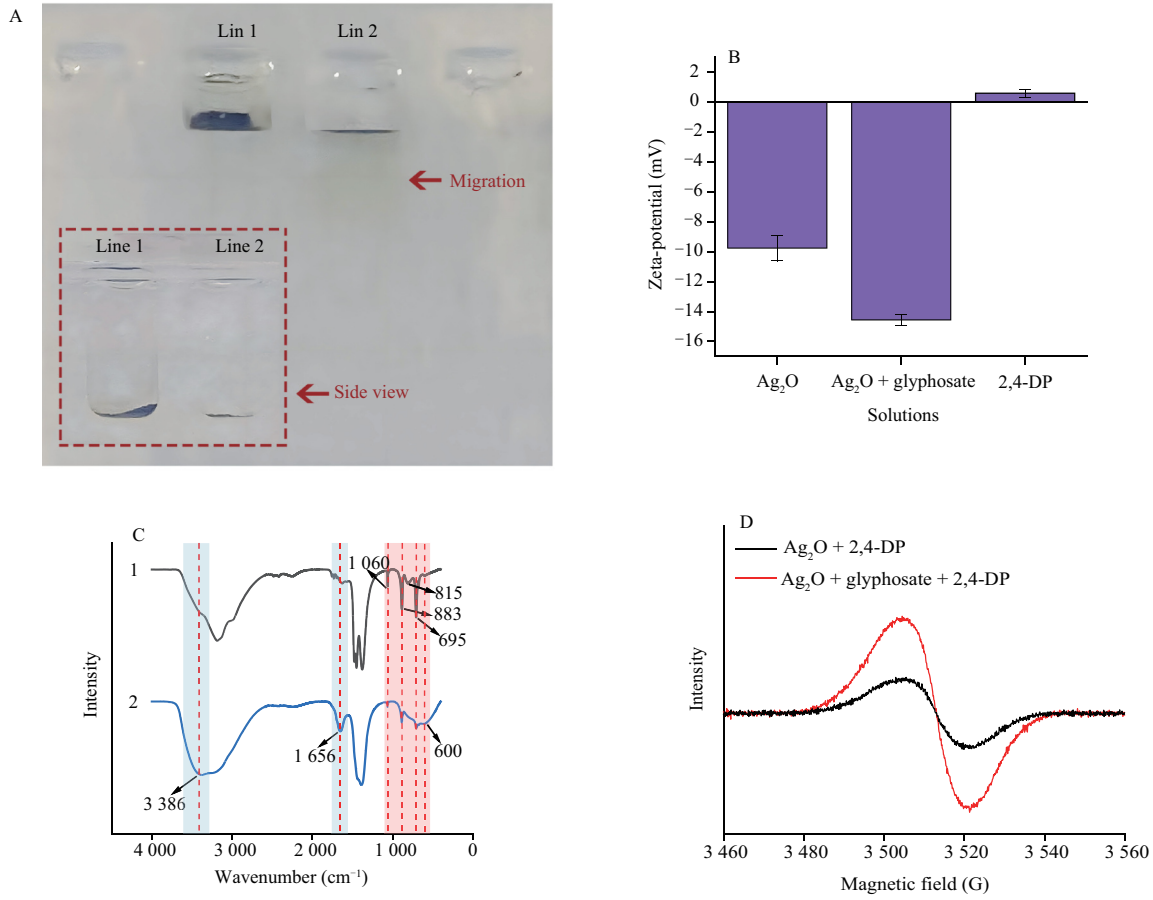

Fig. 4 (A) Agarose gel electrophoresis analysis of the interaction between glyphosate and cubic Ag_2O NPs. Inset: The corresponding sectional photo of the injection holes (side view). (B) Zeta-potential of various solutions pH 7.5. (C) FTIR spectra of different samples. Sample 1, Ag_2O; Sample 2, Ag_2O + glyphosate. (D) EPR spectrum of the radical generated during the catalytic process.

that glyphosate molecules rich in hydroxyl groups were adsorbed onto the surface of Ag_2O. Moreover, the addition of glyphosate changed the intensities of all peaks of Ag–O (1 060, 883, 815, 695 and 600 cm^{-1}), indicating that multiple interaction sites on Ag_2O were altered by glyphosate. Based on the above results and previous reports[51-52], it is reasonable to speculate that glyphosate is mainly adsorbed on the surface of Ag_2O through hydrogen bonding (Fig. S4). Considering the pore like structure (Fig. 1E) and other properties of Ag_2O, we speculate that pore diffusion and even van der Waals forces may also play a role in the adsorption process of glyphosate.

3.3.3 *Free radical analysis*

The phenolic substrate 2,4-DP can produce semiquinone radicals in the course of oxidation process[53] and can be determined by EPR[36-37], which has also been confirmed by previous reports[41,54]. To explore the changes of radicals in the catalytic solution, we measure the spectrum of free radical signals before and after with the adjunction of glyphosate (Fig. 4D). There is an obvious ESR signal appears in the catalytic system of nanozymes, indicating that the cubic Ag_2O NPs indeed can oxidize phenolic 2,4-DP to produce semiquinone radicals. After adding glyphosate, the radical signal peak of the sensing solution is apparently increased. The result indicate that glyphosate can promote the production of semiquinone radicals in the catalytic solution, and then enhance the laccase-like activity of Ag_2O NPs.

3.3.4 *Electrochemical analysis*

To further elucidate the mechanism of enhancing the laccase-like activity, cyclic voltammetry experiments are performed on the reaction system before and after adding glyphosate (Fig. S5). Both individual 2,4-DP solutions and 4-AAP solutions exhibit oxidation peaks at different potentials (Samples 1−2), which suggests that they all electrocatalytic oxidation. The catalytic solution of cubic Ag_2O NPs generates an oxidation peak with a current of 19.59 μA at 0.53 V (Sample 3). The peak location of 2,4-DP is changed, which is due to the Ag_2O NPs promoting the oxidation of substrate and then reacting with chromogenic agent 4-AAP to produce new products. Surprisingly, once various quantities of glyphosate are added, the peak current of the reaction solution increases from 19.59 μA to 24.01 and 33.83 μA (Samples 4−5), respectively. However, individual pesticide molecules cannot be electrocatalytic oxidation (Sample 6). These phenomena demonstrate that the addition of glyphosate accelerates the electron transfer between nanozymes and substrates, thereby promoting the simulated laccase-like activity of Ag_2O NPs.

3.3.5 *Effect of glyphosate on enzymatic kinetics*

The relationship between the quantities of glyphosate and the reaction rate of cubic Ag_2O NPs is revealed through steady-state kinetic analysis. By changing the concentrations of glyphosate and 2,4-DP, Michaelis-Menten curves (Fig. 5A) and double reciprocal curves (Fig. 5B) are obtained, and the apparent kinetic parameters are collected in Table S1. With the contents of glyphosate raises, the maximum reaction rate of Ag_2O gradually increases. However, the K_m value, the affinity of Ag_2O to the substrate, did not change significantly after the addition of glyphosate. It is speculated that the reason may be that the initial rate of the reaction was recorded in the kinetic experiment, and at the beginning of the reaction, the adsorption capacity of glyphosate on Ag_2O is not large enough, so the rapid increase in the adsorption of the substrate has not been captured.

3.4 *Optimization of detection conditions*

3.4.1 *Effect of HEPES*

Many nanozymes typically exhibit strong enzyme activity under acidic circumstances. The influence of pH value and ion content of HEPES buffer on sensor detection is investigated. The results in Fig. S6 show that the constructed sensor obtains the peak value of absorbance value in HEPES with pH 7.5, which indicates that the method can obtain the optimal detection performance in a near-neutral condition. As the buffer amount increases, the sensing signal of the system at 510 nm sharply raises and obtains its maximum value at 15 mmol/L (Fig. S7). If the buffer content is further increased, the absorbance difference of the solution is reduced gradually, which is probably because the high salt ion concentration is not conducive to catalysis of nanozymes.

3.4.2 *Effect of 2,4-DP and 4-AAP concentration*

To obtain the optimum detection circumstances for the established sensor, we also investigate the effects of substrate amounts of 2,4-DP and 4-AAP. As can be seen from Fig. S8, the absorbance difference of sensing system progressively raises with the increase of the phenol 2,4-DP content, and reaches the peak value at 100 μg/mL. Once the quantity of the 2,4-DP continues to increase, the absorbance value of the solution decreases sharply. The reason may be due to the fact that the limited cubic Ag_2O NPs cannot oxidize excessive substrates. When the concentration of 4-AAP is low, the absorbance difference of the system raises rapidly and reaches a maximum value at 100 μg/mL (Fig. S9). If the concentration of 4-AAP is more than 100 μg/mL, the sensor signal nevermore increases, which may be that the 4-AAP bound to the semiquinone radicals has become saturated.

3.4.3 *Effect of nanozyme and temperature*

The content of nanozymes is crucial to the construction of sensors, and we further studied the influence of Ag_2O quantity on detection signals (Fig. S10). As the raise of Ag_2O content, the absorbance value of solution gradually increases until the quantity of nanozyme is 20 μg/mL. The detection signal of the system decreases significantly with the amount of the Ag_2O further increases, which may be due to the limited pesticide molecules could not completely adsorb the excess nanozymes. The Ag_2O solution containing glyphosate is stored at −20 to 80 ℃ for 20 min, and then 2,4-DP, HEPES buffer and 4-AAP are added and thoroughly mixed. The detection signal of the mixed solution is measured to determine the effect of temperature on established sensor (Fig. S11). At −20 to 20 ℃, the absorbance difference increases sharply as the raise of temperature. However, at 20−80 °C, the sensing signal increases slowly. Considering that the constructed sensor has a good detection signal at 20 ℃, we chose to conduct subsequent experiments at room temperature.

3.5 *Sensitivity of sensor*

The sensitivity of glyphosate colorimetric sensor is assessed by analyzing the variation of color, UV/Vis spectrum and sensing signal front and back with adding various concentrations of pesticide to Ag_2O catalytic solution (Fig. 6). The absorbance difference of the solution raises as the increase of glyphosate, and the corresponding color progressively changes from the initial pink to deep red. There is a good linear relationship between the absorbance of the sensor and the concentration of glyphosate

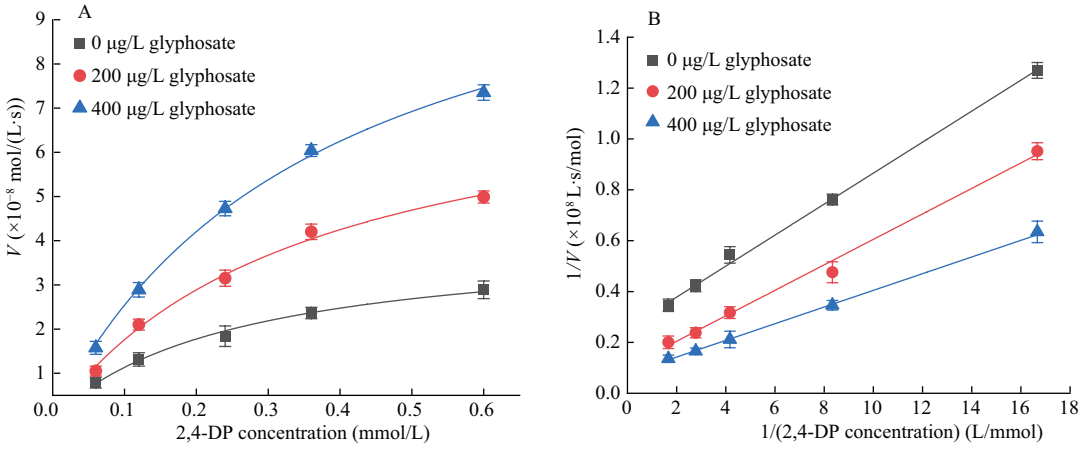

Fig. 5 (A) Michaelis-Menten plots for the oxidation of 2,4-DP catalyzed by cubic Ag_2O NPs in the presence of glyphosate. (B) Lineweaver-Burk plots for the oxidation of 2,4-DP catalyzed by cubic Ag_2O NPs in the presence of glyphosate.

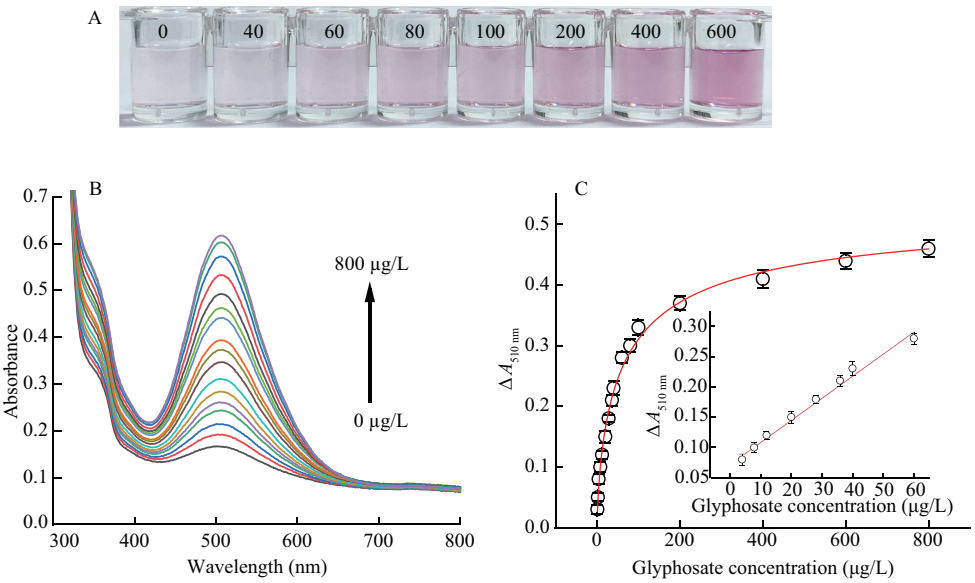

Fig. 6 Visual pictures of the colorimetric sensor with different amounts of glyphosate added. (B) UV/Vis absorbance spectra of the colorimetric sensor treated with varying concentrations of glyphosate. (C) Relationship between absorbance difference (ΔA) and glyphosate content. Inset: absorbance changes of catalytic systems at low quantity of glyphosate ($y = 0.007\,4 + 0.008\,4x$, $R^2 = 0.994$).

between 6 and 60 μg/L. When the content of glyphosate is more than 400 μg/L, the sensing signal and color of the system nevermore change significantly. The calculated limit of detection (LOD)[55] is 2.09 μg/L (12.32 nmol/L), which is well below the maximum limit for glyphosate in food stipulated by various institutions. To evaluate the detection performance of the proposed colorimetric sensor, we compare it with other glyphosate detection methods that have been reported (Table S2). Even though fluorescent and electrochemical methods have lower LODs and wider linear ranges, they often demand cumbersome electrode processing[56], and even fluorescent methods may use toxic substances. In recent years, colorimetric method has been widely concerned by researchers. On the contrary, the colorimetric method can easily and quickly to identify glyphosate without expensive instruments.

Compared with other glyphosate colorimetric sensors, the established sensor using laccase-like activity of nanomaterials has strengths such as being facile, cheap, reliable and sensitive. Notably, laccase does not require H_2O_2 to be involved in the catalytic process, which avoids the inaccurate results induced by the presence of different peroxidases in complicated environment. In addition, most of the reported glyphosate detection methods currently inhibit enzyme activity, and we firstly propose a strategy for detecting glyphosate residues by enhancing the catalytic activity of nanomaterials, which can provide new ideas for the analysis of other pesticides in food.

3.6 *Smartphone-assisted detection of glyphosate*

Because of the correlation between the color change of the sensing solution and glyphosate concentration, and the color is situated in the visible light area, which allows us to establish a standard curve for detecting pesticide quantity relied on RGB values. Firstly, take photos of the reaction system under a fume hood with a fixed light source, and then the data of the photo is converted by the software on the smartphone to obtain the corresponding RGB value. Finally, a standard curve is established using the RGB value of the system and the quantity of glyphosate. The results are shown in Fig. 7, with the concentration of glyphosate increases from 0 to 600 μg/L, the color of the reaction system gradually turns from colorless to pink or even deep red, and the corresponding R/G value also increases. There is a good linear relationship between the R/G value and the concentration of glyphosate (40–200 μg/L). The calculated LOD is 16.2 μg/L (95.48 nmol/L), which is also well below the maximum limit for glyphosate in food stipulated by various institutions. The combination of smartphones can simplify the conventional analysis procedure and can satisfy the on-site monitoring needs of glyphosate in food.

3.7 *Selectivity and stability of sensor*

To evaluate the selectivity of the constructed colorimetric method for glyphosate, various pesticides such as malathion, carbendazim, dimethoate, isocarbophos, paraquat, dichlorvos, parathion-methyl, iprobenfos, trichlorfon, chlorpyrifos, omethoate, acetamiprid, λ-cyhalothrin, and carbaryl are added to the solution (Fig. 8). From the results in the Fig. 8, the reaction system containing other pesticides is pink, while the solution containing glyphosate is dark red. Moreover, the absorbance difference of the sensing solution containing glyphosate pesticide is obviously higher than that of other solutions. Surprisingly, the response of the sensing solution to glyphosate is not disturbed by other pesticides. These results indicate that the proposed colorimetric sensor has high selectivity and good anti-interference capability to glyphosate pesticide. Given that the detection performance of glyphosate colorimetric sensors is closely related to the catalyst, the stability of Ag_2O nanomaterial has been investigated (Fig. S12). Strikingly,

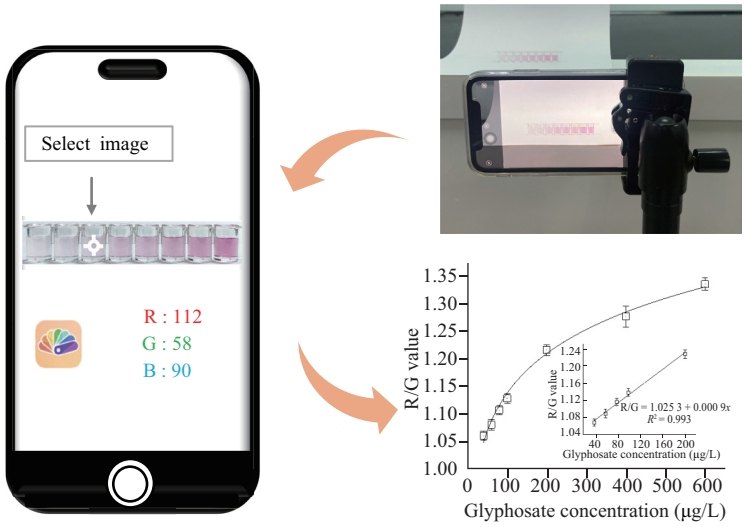

Fig. 7 Procedure of smartphone-assisted detection of glyphosate. Inset: R/G changes of catalytic systems at low quantity of glyphosate (R/G = 1.025 3 + 0.000 9x, R^2 = 0.993).

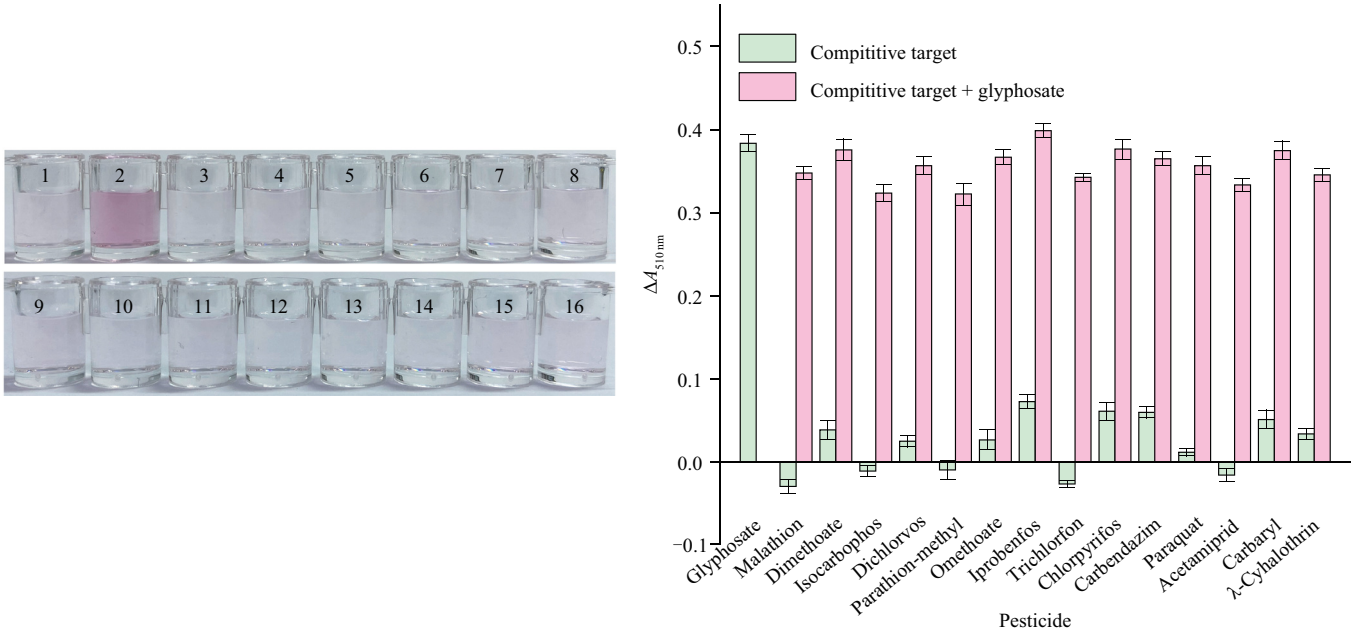

Fig. 8 Visual picture of the colorimetric sensor containing various pesticides, and the consequential absorbance difference. Sample 1: Ag_2O; Samples 2−16: Sample 1 + different pesticides (they are glyphosate, malathion, dimethoate, isocarbophos, dichlorvos, parathion-methyl, omethoate, iprobenfos, trichlorfon, chlorpyrifos, carbendazim, paraquat, acetamiprid, carbaryl and λ-cyhalothrin in order).

the laccase-like activity of Ag_2O remained almost unchanged after 6 months. Moreover, the constructed colorimetric sensor for glyphosate detection also can maintain a relative sensing signal of approximately 94% after 6 months (Fig. S13). Such excellent stability makes the colorimetric sensor potentially suitable for practical applications in various situations.

3.8 Analysis of glyphosate residues in real samples

To evaluate the applicability of the smartphone-assisted colorimetric sensor to glyphosate, various quantities of glyphosate are acceded to three real food samples. The recovery rate is analyzed, and the effectiveness of the detection results is validated through HPLC method (Table 1). The average recovery range of glyphosate is 91.34%−98.71%, and the relative standard deviation (RSD) is 2.9%−5.4%, which is substantially agreement with the data obtained by instrument method. Moreover, we also assess the suitability of the smartphone-assisted colorimetric sensor in real samples, and the results also consistent with the HPLC method. The experimental data suggest that the established smartphone-assisted colorimetric sensor is suitable and accurate, which can be applied to detect glyphosate in real samples in food.

Table 1
Determination of glyphosate in spiked real food samples.

Sample	Spiked*	Colorimetric biosensor			Smartphone-assisted sensor			HPLC		
		Found*	Recovery (%)	RSD (%)	Found*	Recovery (%)	RSD (%)	Found*	Recovery (%)	RSD (%)
Tap water	0	0	None	None	0	None	None	0	None	None
	10	9.74 ± 0.05	97.36	3.2	9.65 ± 0.06	96.50	2.9	9.73 ± 0.04	97.30	2.8
	50	48.22 ± 0.12	96.44	4.2	43.47 ± 0.15	86.93	5.2	47.98 ± 0.13	95.96	4.1
	100	91.34 ± 0.18	91.34	3.3	93.51 ± 0.24	93.51	4.3	96.32 ± 0.21	96.32	3.3
Orange juice	0	0	None	None	0	None	None	0	None	None
	10	9.54 ± 0.09	95.40	4.1	9.11 ± 0.10	91.10	4.7	9.66 ± 0.05	96.60	3.8
	50	47.10 ± 0.15	94.20	5.4	42.45 ± 0.18	84.90	2.8	48.12 ± 0.15	96.24	5.2
	100	94.56 ± 0.21	94.56	2.9	93.40 ± 0.11	93.40	5.1	95.77 ± 0.19	95.77	4.4
Soybean	0	0	None	None	0	None	None	0	None	None
	10	9.68 ± 0.07	96.80	3.4	9.29 ± 0.09	92.90	4.4	9.88 ± 0.07	98.8	5.3
	50	47.32 ± 0.17	94.64	4.1	45.66 ± 0.14	91.32	3.5	48.11 ± 0.16	96.22	4.5
	100	96.45 ± 0.19	96.45	3.6	92.98 ± 0.17	92.98	2.9	97.23 ± 0.20	97.23	3.8
Apple	0	0	None	None	0	None	None	0	None	None
	10	9.77 ± 0.13	97.70	2.9	9.39 ± 0.35	93.90	2.8	9.87 ± 0.17	98.70	3.7
	50	47.10 ± 0.45	94.20	3.2	45.73 ± 0.22	91.46	4.7	48.63 ± 0.24	97.26	4.2
	100	98.71 ± 0.06	98.71	3.8	95.86 ± 0.16	95.86	3.6	98.22 ± 0.32	98.22	3.0
Tea leaf	0	0	None	None	0	None	None	0	None	None
	10	9.358 ± 0.43	93.58	4.2	9.26 ± 0.37	92.60	3.5	9.34 ± 0.34	93.40	4.6
	50	48.92 ± 0.18	97.84	3.7	47.41 ± 0.26	94.82	4.2	45.72 ± 0.42	91.44	2.8
	100	97.11 ± 0.23	97.11	3.6	94.58 ± 0.34	94.58	4.5	94.51 ± 0.11	94.51	3.6

Note: *The unit of glyphosate concentration is expressed in liquid and solid samples in terms of μg/L and μg/kg, respectively.

4 Conclusions

In summary, a facile, reliable and rapid smartphone-assisted colorimetric sensor is established relied on enhancing the laccase-like activity of nanomaterials. The LOD for glyphosate stands at 2.09 μg/L, significantly lower than the maximum allowable content set by the Chinese Ministry of Agriculture for glyphosate in vegetables and fruits, which is 0.5 mg/kg, as well as the maximum limit established by the US Environmental Protection Agency for glyphosate residue in drinking water, which is 700 μg/L. Compared with other detection methods of glyphosate, the constructed colorimetric sensor does not require H_2O_2 to be involved in the detection procedure, which can obtain relatively accurate results of detection from complex food samples. The established sensor can be employed to the rapid determination of glyphosate concentration in tap water, orange juice and other food samples, and the data of detection are consistent with those of instrument method. Moreover, the standard curve of RGB value versus glyphosate quantity is determined by a smartphone. The smartphone-assisted sensor has been successfully employed to the detection of real samples, which can be widely applied to the rapid detection of pesticide residue in food.

Conflict of interest

No conflict of interest exits in the submission of this manuscript, and all authors agreed on this submission.

Acknowledgements

This work was financially supported by the National Natural Science Foundation of China (32360621, 32160603, 31760486), the Guizhou Provincial Basic Research Program (ZK[2021]Key Project 037), the Guizhou Provincial Key Technology R&D Program (QKHZC[2026]318), and the Open Foundation of Key Laboratory of Wuliangye-flavor Liquor Solid-state Fermentation (2023JJ009), China National Light Industry.

Appendix A. Supplementary data

Supplementary data to this article can be found online at https://doi.org/10.26599/FSHW.2024.9250401.

References

[1] Q. Liu, S. Li, Y. Wang, et al., Sensitive fluorescence assay for the detection of glyphosate with NAC-Cu^{2+} complex, Sci. Total Environ. 882 (2023) 163548. https://doi.org/10.1016/j.scitotenv.2023.163548.

[2] Q. Zhang, Z. Zhang, S. Xu, et al., Enzyme-free and rapid visual quantitative detection for pesticide residues utilizing portable smartphone integrated paper sensor, J. Hazard. Mater. 436 (2022) 129320. https://doi.org/10.1016/j.jhazmat.2022.129320.

[3] C.T. Thanh, N.H. Binh, P.N.D. Duoc, et al., Electrochemical sensor based on reduced graphene oxide/double-walled carbon nanotubes/octahedral Fe_3O_4/chitosan composite for glyphosate detection, Bull. Environ. Contam. Toxicol. 106(6) (2021) 1017-1023. https://doi.org/10.1007/s00128-021-03179-7.

[4] M.B. Gholivand, A. Akbari, L. Norouzi, Development of a novel hollow fiber-pencil graphite modified electrochemical sensor for the ultra-trace analysis of glyphosate, Sens. Actuators, B 272 (2018) 415-424. https://doi.org/10.1016/j.snb.2018.05.170.

[5] S. Singh, V. Kumar, S. Datta, et al., Glyphosate uptake, translocation, resistance emergence in crops, analytical monitoring, toxicity and degradation: a review, Environ. Chem. Lett. 18(3) (2020) 663-702. https://doi.org/10.1007/s10311-020-00969-z.

[6] M. Regiart, A. Kumar, J.M. Goncalves, et al., An electrochemically synthesized nanoporous copper microsensor for highly sensitive and selective determination of glyphosate, ChemElectroChem 7(7) (2020) 1558-1566. https://doi.org/10.1002/celc.202000064.

[7] D. Rettke, J. Doering, S. Martin, et al., Picomolar glyphosate sensitivity of an optical particle-based sensor utilizing biomimetic interaction principles, Biosens. Bioelectron. 165 (2020) 112262. https://doi.org/10.1016/j.bios.2020.112262.

[8] G.A.B. Lanzarin, C.A.S. Venancio, S.M. Monteiro, et al., Behavioural toxicity of environmental relevant concentrations of a glyphosate commercial formulation-RoundUp® UltraMax-During zebrafish embryogenesis, Chemosphere 253 (2020) 126636. https://doi.org/10.1016/j.chemosphere.2020.126636.

[9] B.B. Prasad, D. Jauhari, M.P. Tiwari, Doubly imprinted polymer nanofilm-modified electrochemical sensor for ultra-trace simultaneous analysis of glyphosate and glufosinate, Biosens. Bioelectron. 59 (2014) 81-88. https://doi.org/10.1016/j.bios.2014.03.019.

[10] A. Steinborn, L. Alder, B. Michalski, et al., Determination of glyphosate levels in breast milk samples from Germany by LC-MS/MS and GC-MS/MS, J. Agric. Food Chem. 64(6) (2016) 1414-1421. https://doi.org/10.1021/acs.jafc.5b05852.

[11] E. Okada, T. Coggan, T. Anumol, et al., A simple and rapid direct injection method for the determination of glyphosate and AMPA in environmental water samples, Anal. Bioanal. Chem. 411(3) (2019) 715-724. https://doi.org/10.1007/s00216-018-1490-z.

[12] B. Wimmer, M. Pattky, L.G. Zada, et al., Capillary electrophoresis-mass spectrometry for the direct analysis of glyphosate: method development and application to beer beverages and environmental studies, Anal. Bioanal. Chem. 412(20) (2020) 4967-4983. https://doi.org/10.1007/s00216-020-02751-0.

[13] R. Xu, S. Dai, M. Dou, et al., Simultaneous, label-free and high-throughput SERS detection of multiple pesticides on Ag@three-dimensional silica photonic microsphere array, J. Agric. Food Chem. 71(6) (2023) 3050-3059. https://doi.org/10.1021/acs.jafc.2c07846.

[14] F. Zhao, D. Guo, X. Tang, et al., Ratiometrically electrochemical and colorimetric dual-mode detection of glyphosate based on 2D Cu-TCPP(Fe) NSs, Talanta 267 (2024) 125207. https://doi.org/10.1016/j.talanta.2023.125207.

[15] Y. Yuan, J. Jiang, S. Liu, et al., Fluorescent carbon dots for glyphosate determination based on fluorescence resonance energy transfer and logic gate operation, Sens. Actuators, B 242 (2017) 545-553. https://doi.org/10.1016/j.snb.2016.11.050.

[16] M. Narayanan, A. Amalraj, P. Perumal, A copper oxide functionalized neodymium oxide hybrid nanostructure interconnected with modified glassy carbon electrode (CuO–Nd_2O_3/GCE) for electrochemical determination of Malathion pesticide, J. Mater. Res. 38(2) (2023) 416-428. https://doi.org/10.1557/s43578-022-00826-5.

[17] C. Jiang, H. Zhong, J. Zou, et al., CuCeTA nanoflowers as an efficient peroxidase candidate for direct colorimetric detection of glyphosate, J. Mater. Chem. B 11(40) (2023) 9630-9638. https://doi.org/10.1039/d3tb01455j.

[18] R. Jesuraj, A. Amalraj, V.K. Vaidyanathan, et al., Exceptional peroxidase-like activity of an iron and copper based organic framework nanosheet for consecutive colorimetric biosensing of glucose and kanamycin in real food samples, Analyst 148(20) (2023) 5157-5171. https://doi.org/10.1039/D3AN01242E.

[19] X. Niu, H. He, H. Ran, et al., Rapid colorimetric sensor for ultrasensitive and highly selective detection of fumonisin B_1 in cereal based on laccase-mimicking activity of silver phosphate nanoparticles, Food Chem. 429 (2023) 136903. https://doi.org/10.1016/j.foodchem.2023.136903.

[20] M. Javed, A. Matloob, F.E. Ettoumi, et al., Novel nanobubble technology in food science: application and mechanism, Food Innovation Adv. 2(2) (2023) 135-144. https://doi.org/10.48130/fia-2023-0014.

[21] H. Zhang, W.K. Kang, Y. Wang, et al., An enzymatic reaction modulated fluorescence-on omethoate biosensor based on Fe_3O_4@GO and copper nanoparticles, J. Anal. Test. 6(1) (2022) 3-11. https://doi.org/10.1007/s41664-022-00210-6.

[22] W. Zou, Y. Tang, H. Zeng, et al., Porous Co_3O_4 nanodisks as robust peroxidase mimetics in an ultrasensitive colorimetric sensor for the rapid detection of multiple heavy metal residues in environmental water samples, J. Hazard. Mater. 417 (2021) 125994. https://doi.org/10.1016/j.jhazmat.2021.125994.

[23] Y. Tang, X. Huang, X. Wang, et al., G-quadruplex DNAzyme as peroxidase mimetic in a colorimetric biosensor for ultrasensitive and selective detection of trace tetracyclines in foods, Food Chem. 366 (2022) 130560. https://doi.org/10.1016/j.foodchem.2021.130560.

[24] A. Amalraj, M. Narayanan, P. Perumal, Highly efficient peroxidase-like activity of a metal–oxide-incorporated CeO_2–MIL(Fe) metal–organic framework and its application in the colorimetric detection of melamine and mercury ions *via* induced hydrogen and covalent bonds, Analyst 147(14) (2022) 3234-3247. https://doi.org/10.1039/D2AN00864E.

[25] Y. Xu, J. Yan, Y. Zhu, et al., Self-cascade nanoenzyme of cupric oxide nanoparticles (CuO NPs) induced in situ catalysis formation of polyelectrolyte as template for the synthesis of near-infrared fluorescent silver nanoclusters and the application in glutathione detection and bioimaging, Anal. Chem. 94(42) (2022) 14642-14651. https://doi.org/10.1021/acs.analchem.2c02832.

[26] K. Abnous, N.M. Danesh, M. Ramezani, et al., A colorimetric gold nanoparticle aggregation assay for malathion based on target-induced hairpin structure assembly of complementary strands of aptamer, Microchim. Acta 185(4) (2018) 216. https://doi.org/10.1007/s00604-018-2752-3.

[27] H. Zhu, B. Liu, M. Wang, et al., Amorphous Fe-containing phosphotungstates featuring efficient peroxidase-like activity at neutral pH: toward portable swabs for pesticide detection with tandem catalytic amplification, Anal. Chem. 95(10) (2023) 4776-4785. https://doi.org/10.1021/acs.analchem.3c00008.

[28] S. Riva, Laccases: blue enzymes for green chemistry, Trends Biotechnol. 24(5) (2006) 219-226. https://doi.org/10.1016/j.tibtech.2006.03.006.

[29] Y. Lin, F. Wang, J. Yu, et al., Iron single-atom anchored N-doped carbon as a'laccase-like' nanozyme for the degradation and detection of phenolic pollutants and adrenaline, J. Hazard. Mater. 425 (2022) 127763. https://doi.org/10.1016/j.jhazmat.2021.127763.

[30] A.D. Moreno, D. Ibarra, M.E. Eugenio, et al., Laccases as versatile enzymes: from industrial uses to novel applications, J. Chem. Technol. Biotechnol. 95(3) (2020) 481-494. https://doi.org/10.1002/jctb.6224.

[31] H. Li, S. Guo, C. Li, et al., Tuning laccase catalytic activity with phosphate functionalized carbon dots by visible light, ACS Appl. Mater. Interfaces 7(18) (2015) 10004-10012. https://doi.org/10.1021/acsami.5b02386.

[32] L. Wang, Z. Liu, L. Yao, et al., A bioinspired single-atom Fe nanozyme with excellent laccase-like activity for efficient aflatoxin B_1 removal, Small (2024) 2400629. https://doi.org/10.1002/smll.202400629.

[33] M. Li, Y. Xie, L. Lei, et al., Colorimetric logic gate for protamine and trypsin based on the Bpy-Cu nanozyme with laccase-like activity, Sens. Actuators, B 357 (2022) 131429. https://doi.org/10.1016/j.snb.2022.131429.

[34] X. Wang, H.F. Wu, Q. Kuang, et al., Shape-dependent antibacterial activities of Ag_2O polyhedral particles, Langmuir 26(4) (2010) 2774-2778. https://doi.org/10.1021/la9028172.

[35] X. Zhan, Y. Tang, Y. Liu, et al., A novel colorimetric strategy for rapid detection of dimethoate residue in vegetables based on enhancing oxidase-mimicking catalytic activity of cube-shape Ag_2O particles, Sens. Actuators, B 361 (2022) 131720. https://doi.org/10.1016/j.snb.2022.131720.

[36] J. Yuasa, S. Yamada, S. Fukuzumi, Direct EPR detection of a hydrogen-bonded complex between a semiquinone radical anion and a protonated amino acid, and electron transfer driven by hydrogen bonding, Angew. Chem., Int. Ed. Engl. 46(19) (2007) 3553-3555. https://doi.org/10.1002/anie.200700157.

[37] R.V. Barbehenn, U. Poopat, B. Spencer, Semiquinone and ascorbyl radicals in the gut fluids of caterpillars measured with EPR spectrometry, Insect Biochem. Mol. Biol. 33(1) (2003) 125-130. https://doi.org/10.1016/s0965-1748(02)00183-2.

[38] Y. Wang, C. He, W. Li, J. Zhang, et al., Catalytic performance of oligonucleotide-templated Pt nanozyme evaluated by laccase substrates, Catal. Lett. 147(8) (2017) 2144-2152. https://doi.org/10.1007/s10562-017-2106-5.

[39] L. Wang, Y. Bi, J. Gao, et al., Carbon dots based turn-on fluorescent probes for the sensitive determination of glyphosate in environmental water samples, RSC Adv. 6(89) (2016) 85820-85828. https://doi.org/10.1039/c6ra10115a.

[40] R. Bala, A. Swami, I. Tabujew, et al., Ultra-sensitive detection of malathion using quantum dots-polymer based fluorescence aptasensor, Biosens. Bioelectron. 104 (2018) 45-49. https://doi.org/10.1016/j.bios.2017.12.034.

[41] L. Huang, Y. Tang, J. Wang, et al., Cubic Ag_2O nanoparticles as robust laccase mimetics in a smartphone-assisted colorimetric sensor for rapid and ultrasensitive detection of kanamycin in environment, Sens. Actuators, B 391 (2023) 134052. https://doi.org/10.1016/j.snb.2023.134052.

[42] S. Torabi, M.J.K. Mansoorkhani, A. Majedi, et al., Review: synthesis, medical and photocatalyst applications of nano-Ag_2O, J. Coord. Chem. 73(13) (2020) 1861-1880. https://doi.org/10.1080/00958972.2020.1806252.

[43] L. Wang, Y. Bi, J. Hou, et al., Facile, green and clean one-step synthesis of carbon dots from wool: application as a sensor for glyphosate detection based on the inner filter effect, Talanta 160 (2016) 268-275. https://doi.org/10.1016/j.talanta.2016.07.020.

[44] S. Haq, W. Rehman, M. Waseem, et al., Fabrication of pure and moxifloxacin functionalized silver oxide nanoparticles for photocatalytic and antimicrobial activity, J. Photochem. Photobiol., B 186 (2018) 116-124. https://doi.org/10.1016/j.jphotobiol.2018.07.011.

[45] S. Sagadevan, S.F. Alshahateet, J.A. Lett, et al., Highly efficient photocatalytic degradation of methylene blue dye over Ag_2O nanoparticles under solar light irradiation, Inorg. Chem. Commun. 148 (2023) 288. https://doi.org/10.1016/j.inoche.2022.110288.

[46] N. El Messaoudi, A. El Mouden, Y. Fernine, et al., Green synthesis of Ag_2O nanoparticles using Punica granatum leaf extract for sulfamethoxazole antibiotic adsorption: characterization, experimental study, modeling, and DFT calculation, Environ. Sci. Pollut. Res. 30(34) (2023) 81352-81369. https://doi.org/10.1007/s11356-022-21554-7.

[47] K. Kayed, M. Issa, H. Al-Ourabi, The FTIR spectra of Ag/Ag_2O composites doped with silver nanoparticles, J. Exp. Nanosci. 19(1) (2024) 6227. https://doi.org/10.1080/17458080.2024.2336227.

[48] M. Xu, L. Han, S. Dong, Facile fabrication of highly efficient g-C_3N_4/Ag_2O heterostructured photocatalysts with enhanced visible-light photocatalytic activity, ACS Appl. Mater. Interfaces 5(23) (2013) 12533-12540. https://doi.org/10.1080/17458080.2024.2336227.

[49] W.H. Al-Qahtani, G. Murugadoss, K. Narthana, et al., Structural, morphological, optical and electrochemical characterization of Ag_2O/ZnO and ZnO/Ag_2O nanocomposites, J. Ovonic Res. 18(2) (2022) 187-194. https://doi.org/10.15251/jor.2022.182.187.

[50] A. Allwar, M. Herawati, F.S. Wardana, et al., Composite of Ag_2O-CuO/biochar as an adsorbent for removal of amoxicillin and paracetamol from aqueous solution, Int. J. Environ. Sci. Technol. 20(12) (2023) 13411-13422. https://doi.org/10.1007/s13762-023-04922-9.

[51] H.A. Pereira, P.R.T. Hernandes, M.S. Netto, et al., Adsorbents for glyphosate removal in contaminated waters: a review, Environ. Chem. Lett. 19(2) (2021) 1525-1543. https://doi.org/10.1007/s10311-020-01108-4.

[52] A. Feis, C. Gellini, M. Ricci, et al., Surface-enhanced Raman scattering of glyphosate on dispersed silver nanoparticles: a reinterpretation based on model molecules, Vib. Spectrosc. 108 (2020) 103061. https://doi.org/10.1016/j.vibspec.2020.103061.

[53] A. Li, H. Li, Y. Ma, et al., Bioinspired laccase-mimicking catalyst for on-site monitoring of thiram in paper-based colorimetric platform, Biosens. Bioelectron. 207 (2022) 114199. https://doi.org/10.1016/j.bios.2022.114199.

[54] L. Xia, J. Han, X. Huang, et al., Colorimetric sensor and visual enzyme sheets for sensitive detection of dimethoate residue in vegetables based on laccase-like activity of coral-like silver citrate, Food Control 158 (2024) 110252. https://doi.org/10.1016/j.foodcont.2023.110252.

[55] Y. Tang, Y. Hu, Y. Yang, et al., A facile colorimetric sensor for ultrasensitive and selective detection of Lead(II) in environmental and biological samples based on intrinsic peroxidase-mimic activity of WS_2 nanosheets, Anal. Chim. Acta 1106 (2020) 115-125. https://doi.org/10.1016/j.aca.2020.01.043.

[56] Y. Sun, Y. Zhang, H. Zhang, et al., Integrating highly efficient recognition and signal transition of g-C_3N_4 embellished Ti_3C_2 MXene hybrid nanosheets for electrogenerated chemiluminescence analysis of protein kinase activity, Anal. Chem. 92(15) (2020) 10668-10676. https://doi.org/10.1021/acs.analchem.0c01776.